Journal of Membrane Science 323 (2008) 67–76

Contents lists available at ScienceDirect

Journal of Membrane Science

journal homepage: www.elsevier.com/locate/memsci

Critical flux of hard sphere suspensions in crossflow filtration: Hydrodynamic force bias Monte Carlo simulations

Albert S. Kim*, Yuewei Liu

Civil and Environmental Engineering, University of Hawaii at Manoa, 2540 Dole Street, Honolulu, HI 96822, USA

ARTICLE INFO

Article history:
Received 5 December 2007
Received in revised form 4 June 2008
Accepted 5 June 2008
Available online 20 June 2008

Keywords:
Critical flux
Force bias Monte Carlo
Shear-induced diffusion
Phase transition
Order parameter

ABSTRACT

A Monte Carlo method is developed for crossflow membrane filtration to determine the critical flux of hard sphere suspensions. Brownian and shear-induced diffusion are incorporated into an effective hydrodynamic force exerted on the hard spheres in a concentrated shear flow. Effects of shear rate and particle size on the critical flux are investigated using hydrodynamic force bias Monte Carlo simulations, providing a baseline of the critical flux.

1. Introduction

After first noted as the "threshold flux" by Cohen and Probstein [1], the concept of critical flux, defined as "a flux below which a decline of flux with time does not occur; above it fouling is observed" was proposed by Field et al. [2], and the concept was widely adopted in membrane research and development communities. The critical flux is in general dichotomized into two forms: strong and weak. The strong form indicates the flux at which the transmembrane pressure starts deviating from the pure water line of Darcy's law, and/or the first flux for which irreversible fouling appears on the membrane surface. The weak form assumes rapid initial fouling, which brings forth the flux versus transmembrane pressure (TMP) relationship located below the pure water line with a lesser inclination. A rigorous analysis of the critical flux concept can be found in Bacchin et el.'s recent review [3] in terms of the state-of-the-art theory, experiments, and applications.

Near the membrane surface, fouling (regardless whether it is reversible or irreversible) occurs roughly in the following sequential manner: first, pressure forces the solvent to flow through the membrane, generating the permeate flux; second, the permeate flux pushes solutes from the bulk phase to the vicinity of the membrane, causing a biased concentration profile described as the concentration polarization; and third, the gradient of solute concentration engenders solute back diffusion toward the bulk phase, mitigating the boundary layer resistance to reach a balanced state of mass transport. From this viewpoint, the critical flux in colloidal filtration can be basically interpreted as the flux above which the solute back-diffusion is severely suppressed by hydrodynamics while heavy deposition contributes to forming thick cake layers. Following this basic idea, both the strong and weak forms of the critical flux are closely related to diffusion processes, but each flux form with a different initial fouling status may modify the magnitude of the critical flux under the influence of physical and chemical conditions.

It is well known that three back-transport mechanisms play important roles in the critical flux in terms of particle sizes: Brownian diffusion [4], shear-induced diffusion [5–7], and inertial lift [8–13]. For particles ranging from 10 nm to 10 μm, Brownian and shear-induced diffusion are dominant for small and large particles, respectively. Particle sizes falling into the border between Brownian and shear-induced diffusion rage from 0.1 to 1 μm, and their critical fluxes are generally subject to the shear rate. The inertial lift is important for buoyant particles larger than around 10 μm, but their significance may be questionable due to the magnitude of imposing gravitational force if the particle buoyancy is violated.

In addition, Bacchin et al. [14] proposed that the critical flux stems from the repulsive interaction between membrane and particles, which, if subdued, allows particle accumulation/coagulation on the membrane surface, initiating severe (irreversible) fouling. While the significance of Brownian and shear-induced diffusion

* Corresponding author. Tel.: +1 808 956 3718; fax: +1 808 956 5014.
E-mail address: AlbertSK@hawaii.edu (A.S. Kim).
URL: http://pam.eng.hawaii.edu (A.S. Kim).

0376-7388/$ – see front matter © 2008 Elsevier B.V. All rights reserved.
doi:10.1016/j.memsci.2008.06.029

mechanisms were separately investigated [15,16], Sethi and Wiesner [17] assumed the superposition of Brownian and shear-induced diffusivities and studied the transient behavior of permeate flux decline. These theoretical investigations can provide a good understanding of the filtration phenomena within the model scopes and their mathematical approximations. Until this time, the critical flux was barely investigated at a microscopic level for colloidal particles explicitly undergoing both Brownian and shear-induced diffusion.

In experiments, determination or estimation of critical flux is based on observing transient flux change by increasing pressure in a step-wise manner, followed by careful investigation of pressure increase while the permeate flux is kept unchanged [18,19]. Using this method, the critical flux that immediately causes noticeable fouling can be (experimentally) well identified, although the long-term critical flux requires longer testing time in steady-state filtration. In this light, it is desirable to have a microscopic physical quantity at the level of individual particle dynamics, to which the (macroscopic) critical flux can be linked. Many-body interfacial phenomena can be fundamentally scrutinized with simple, basic cases to associate the discrete microscopic events with a continuum macroscopic theory; and then to disclose main origins and properties of the critical flux, which are verified experimentally.

Currently, researchers are studying colloidal membrane filtration using the hydrodynamic force bias Monte Carlo (HFBMC) method [20,21], starting with a copious review of statistical simulation methods [22], applying HFBMC to a dead-end membrane filtration system [23], and dealing with principal issues of HFBMC application to crossflow filtration systems [24]. These prior studies focused on development, modification, and application of HFBMC on colloidal filtration to investigate the deposition structure of particles on the membrane surface, as summarized below. In dead-end filtration simulations [23], applied pressure was assumed to be constant, and transient permeate flux was investigated while interacting particles deposited on the membrane surface and formed cake layer that produced noticeable hydraulic resistance. Particles within the cake layer of a certain volume fraction (which can vary along the normal direction to the membrane surface) undergo remarkable drag forces determined using Happel's correction factor [25]. In addition, a phase transition from liquid-like concentration polarization to solid-like cake layer was delineated by particle volume fraction, identified as the contact between two nearest particles, and used to characterize its link to the critical flux. In our recent work [24], Monte Carlo simulation was firstly applied to a crossflow filtration system, and its modeling issues were extensively discussed in many aspects such as dynamics, deposition and accumulation of particles in an open system, spatial and temporal variations of cake structures, and back-diffusion of colloidal particles. Extending the scope of our previous work, the present study develops a novel Monte Carlo method by updating the tangential bias stemming from the crossflow field and uses the normal bias based on the effective hydrodynamic drag force under a shear flow.

Shear-induced diffusion can be relatively less important than Brownian diffusion when particles are below submicron-size and/or strongly repulsive so that the average interparticle distance between nearest neighbors is (much) more than an order of particle diameter. It is phenomenologically well known that the shear-induced diffusivity is proportional to the square of the volume fraction for low concentrations [7]. For hard spheres, the original shear-induced diffusion should be considered more seriously when a strong shear is imposed in the membrane channel due to a fast crossflow velocity. The absolute shear rate (rather than the crossflow Reynolds number [1]) is the more important primary factor that can efficiently control fouling behavior given the height (or diameter) of the membrane channel. This is because particles go through random displacement, deviating from streamlines in a shear flow, as they hydrodynamically interact with and also tumble over other particles. An analytical expression of effective force acting on a hard sphere undergoing both Brownian and shear-induced diffusion in a concentrated system was recently developed [26], which will be recapitulated in Section 2. In our previous work [26], an irreversible chemical potential was introduced as a non-equilibrium molar Gibb's free energy and used to build a common thermodynamic origin for Brownian and shear-induced diffusion. The third mass transport mechanism, inertial lift, was excluded in our previous paper [26]. The theoretical validity of the inertial lift phenomena during the crossflow MF and UF is entirely based on the single particle trajectory so that its physical origin does not include many-body behaviors of the collective transport. In the regime of particle size where the inertial lift is important ($a \geq 10\,\mu m$), particles are not always neutrally buoyant due to specific gravity (typically greater than 1). As a result, the gravitational influence is not completely cancelled with the buoyant force; and particle migration [13,8] on the permeable or impermeable surface may be a much more important mechanism than diffusion mainly for the large (sub-millimeter) particles.

The current literature lacks studies on microscopic investigations of the critical flux during colloidal filtration, especially as influenced by shear-induced diffusion. In this light, to identify the critical flux in terms of the particle size and shear rate, we chose a model filtration system consisting of non-interacting hard spheres in a fast crossflow and performed the HFBMC simulations. We then examined dynamic particle structures associated with the critical flux and compared MC simulation results with reported experimental observations.

2. Method of biased Monte Carlo simulation

2.1. Canonical Monte Carlo

The HFBMC simulation [23,24] is used to mimic steady-state structures of colloidal (hard sphere) suspensions near critical flux ranges, given a set of operating conditions. Biased transition probability in MC simulations is composed of tangential (axial) and normal (vertical) components, which are implemented separately due to the different orders of magnitudes between the crossflow velocity and permeate flux. Canonical ensemble, in which the total number of particles, representative volume, and temperature are constant, is used in practice to simulate the particle distribution within the membrane channel.

2.1.1. Initial setting

To investigate the critical flux of hard sphere suspensions with respect to particle size (diameter) and shear rate of the crossflow, a small section of the entire crossflow channel is selected as a representative volume, denoted in this study as a simulation box as shown in Fig. 1. The simulation starts with the initial random positioning of N_p particles in the box of dimension $L \times W \times H$, where $L(=3W)$, W, and $H(=7W)$ are the length, width, and height of the membrane channel, respectively. The length is set three times of the width to clearly inspect axial transport of particles in the crossflow direction, and the height is set seven times of the width to emphasize the concentration polarization and cake formation in the direction normal to the membrane surface. An initial volume fraction ϕ_{ini} is arbitrarily assigned, e.g., 0.1 – greater than typical feed volume fraction ϕ_{feed} of orders of $O(10^{-3} - 10^{-5})$ – to allow for faster convergence of the spatial configuration of particles to a dynamic equilibrium state. With an educated guess of ϕ_{ini}, a dynamic equilibrium configuration yields a solid-like dense structure on the membrane surface and a liquid-like solution phase

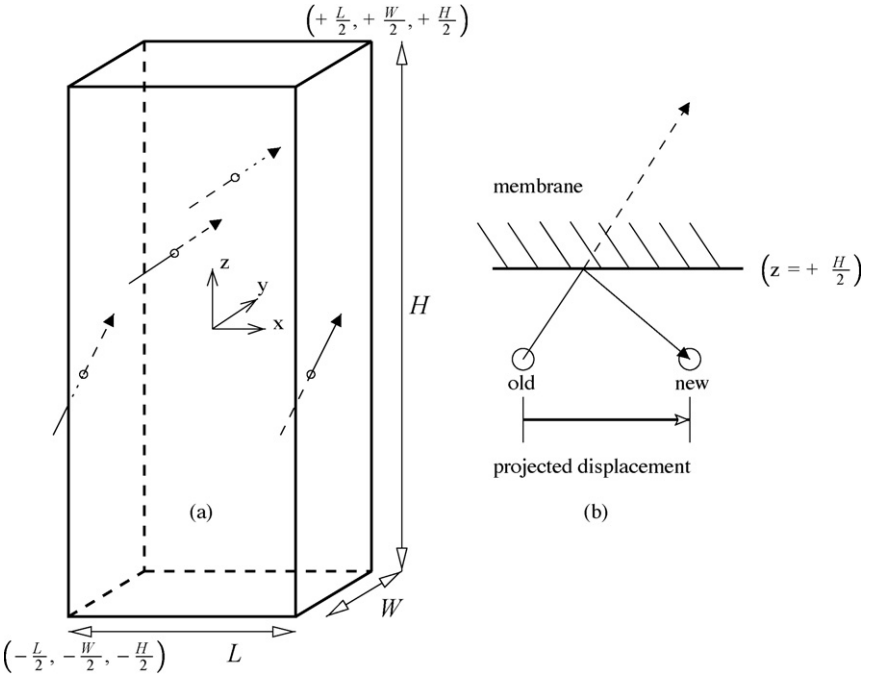

Fig. 1. The simulation box as a representative volume, showing (a) periodic boundary conditions in the x- and y-directions, and (b) reflecting boundary condition in the z-direction.

(representing feed suspension) near the channel epicenter. The width of the simulation box is determined using

$$(W)(3W)(7W) = \frac{N_p(4\pi/3)a^3}{\phi_{\text{ini}}} \tag{1}$$

where a is the particle radius. At the beginning of the simulation, all the particles are randomly located at

$$-\left(\frac{L}{2} - a\right) < x < +\left(\frac{L}{2} - a\right) \tag{2a}$$

$$-\left(\frac{W}{2} - a\right) < y < +\left(\frac{W}{2} - a\right) \tag{2b}$$

$$-\left(\frac{H}{2} - a\right) < z < +\left(\frac{H}{2} - a\right) \tag{2c}$$

avoiding any overlap between two particles.

In the x- and y-directions, the periodic boundary condition is used to mimic spatial homogeneity: a particle exiting the boundary at $x = +L/2$ returns to the opposite side boundary at $x = -L/2$, and the same as in the y-direction as shown in Fig. 1(a). The periodic boundary condition in the x-direction implicitly assumes that in the simulation box the thickness of the concentration polarization layer or cake layer is locally constant along the crossflow direction. The boundary condition in the y-direction (perpendicular to the crossflow direction) indicates the absence of wall effects. If a particle escapes in the positive z-direction, it returns back to the interior of the membrane channel as shown in Fig. 1(b) and moves in the x–y plane as much as the projected displacement from the old position; and the same boundary condition is also applied in the negative z-direction. Another possible way is to let the particle stay at the old position if the new position suggested is out of the simulation box, but this reflecting boundary condition used can enhance the translation of particles in the x–y plane near the membrane surfaces and therefore speed up reaching a dynamic equilibrium state of particle configuration.

This model, based on a representative simulation box, estimates the mean field approximation using the axial average of flow field, permeate flux, and concentration variation. To conceptually validate this model, the position of the representative box must be located in the middle of the membrane channel, where the local permeate flux is (about) equal to the length-averaged permeate flux. For future research, it would be possible to make a long series of the representative boxes along the direction of the crossflow, exchange the information of particle transport, and investigate the axial variation of permeate flux, pressure, and concentration polarization followed by cake formation. This kind of work requires parallel computing using many processors communicating through Message Passing Interface (MPI) [27].

2.1.2. Ambient flow field

The ambient flow field is based upon Berman's work [28] on laminar flow in channels with porous walls, which can be readily applied to the crossflow membrane filtration. Using the perturbation technique, Berman derived

$$u(x,\eta) = \bar{u}\left[1 - \frac{v_w x}{\bar{u}h}\right]\left[\frac{3}{2}(1-\eta^2)\right]\left[1 - \frac{Re}{420}(2 - 7\eta^2 - 7\eta^7)\right] \tag{3a}$$

$$v(\eta) = v_w\left[\frac{\eta}{2}(3-\eta^2) - \frac{Re}{280}\eta(2 - 3\eta^2 + \eta^6)\right] \tag{3b}$$

with

$$\eta = \frac{z}{h} \tag{4}$$

where u and v are velocity components in the x- and y-directions, respectively, v_w is the constant permeate velocity, $h(= H/2)$ is the channel half-height, and Re is the permeate Reynolds number defined as

$$Re = \frac{v_w h}{\nu} \tag{5}$$

where ν is the kinematic viscosity. By taking values of $v_w = \mathrm{O}(10^{-5} - 10^{-6})$ m/s, $h = \mathrm{O}(10^{-2} - 10^{-3})$ m, and $\nu \simeq 10^{-6}\,\mathrm{m^2/s}$ which are typical in crossflow filtration, we neglect terms with the Reynolds number in u and v of Eq. (3) because Re ranges from 10^{-3}

to 10^{-1} and its denominators are of the order of $O(10^2)$, and then assume

$$\frac{v_w l}{\bar{u}h} \ll 1 \tag{6}$$

where l is the membrane length. The final form of the ambient velocity within the simulation box is approximated as

$$u(\eta) \simeq \bar{u}\frac{3}{2}(1-\eta^2) \tag{7a}$$

$$v(\eta) \simeq v_w \frac{1}{2}\eta(3-\eta^2) \tag{7b}$$

where $\bar{u}$ is the average crossflow velocity. The shear rate at a dimensionless distance η from the membrane surface is calculated as

$$\dot{\gamma}(\eta) = \frac{1}{h}\frac{\mathrm{d}u}{\mathrm{d}\eta} = -\eta\frac{3\bar{u}}{h} \tag{8}$$

which reaches its maximum (in magnitude) on the membrane surfaces (i.e., $\eta = \pm 1$) and vanishes near the channel epicenter (i.e., $\eta \simeq 0$).

2.1.3. Biased transition probability

2.1.3.1. Tangential bias. It is assumed that particle movement is highly subject to the ambient crossflow field in the tangential (x-)direction, characterized by crossflow Peclet number uh/D_0 where D_0 is the Stokes–Einstein diffusivity. For instance, at the epicenter of the membrane channel (i.e., $z = 0$), particle transport is fully convection-dominated (minimally influenced by Brownian motion), and hence the movement occurs mostly in the positive x-direction. Near the membrane surface, however, the no-slip boundary condition provides an environment in which diffusion is not negligible. Comparing typical values of crossflow velocity of an order of $O(10^{-1} - 10^{0})$ and permeate velocity of $O(10^{-5} - 10^{-6})$ indicates that the local Peclet number at the epicenter is 10^4 to 10^6 times greater than that on the membrane surface. Considering dominant transport mechanisms in terms of the local Peclet number at different vertical locations, the random displacement of each particle (from an old position $\mathbf{r}_{\mathrm{old}}$ to a new position $\mathbf{r}_{\mathrm{new}}$) is assigned as

$$\Delta x = x_{\mathrm{new}} - x_{\mathrm{old}} = a_0(2 \times \mathrm{rand} - 1 + P_x) \tag{9a}$$

$$\Delta y = y_{\mathrm{new}} - y_{\mathrm{old}} = a_0(2 \times \mathrm{rand} - 1) \tag{9b}$$

$$\Delta z = z_{\mathrm{new}} - z_{\mathrm{old}} = a_0(2 \times \mathrm{rand} - 1) \tag{9c}$$

where a_0 is the (positive) maximum displacement of the random movement (adjusted during the simulation to maintain the acceptance ratio of the random transition close to 0.5 [29]), rand is the random number (between 0.0 and 1.0) generated using the intrinsic FORTRAN 90 function, `rand`, and P_x is the transition probability of axial bias, which readily includes the crossflow influence on particle movement:

$$P_x = \frac{u(\eta)}{u(\eta = 0)} = 1 - \eta^2 \tag{10}$$

and hence,

$$\Delta x = x_{\mathrm{new}} - x_{\mathrm{old}} = a_0(2 \times \mathrm{rand}) \ \text{ at } \ \eta = 0(\text{epicenter}) \tag{11a}$$

$$\Delta x = x_{\mathrm{new}} - x_{\mathrm{old}} = a_0(2 \times \mathrm{rand} - 1) \ \text{ at } \ \eta = \pm 1(\text{surfaces}) \tag{11b}$$

As shown in Fig. 2, near the epicenter of the channel, particles are allowed to move only in the crossflow direction: the transition probability in the $+x$ and $-x$ directions are 1.0 and 0.0, respectively. On the membrane surface, however, particles can almost randomly move in either direction, even against the crossflow: the transition probability in $+x$ and $-x$ directions are commonly 0.5. Actual

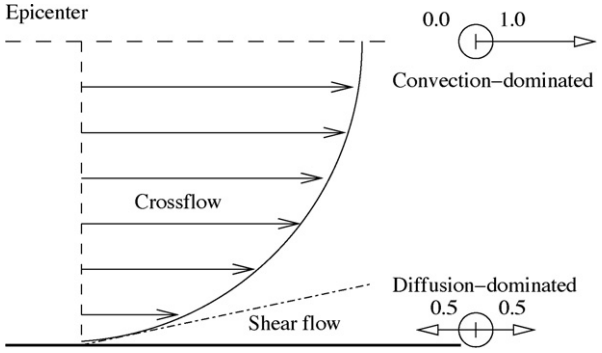

Fig. 2. Dominant transport mechanism at different locations within the membrane channel: the axial bias stemming from the flow profile.

transition of a particle from an old to a new position is mainly subject to interparticle overlap. P_x only contributes to proposing new positions being biased toward the crossflow.

2.1.3.2. Normal bias. Since the main goal of this study is to determine critical flux of hard-sphere suspensions, the permeate flux is set at a constant, resembling the constant flux operation, and dynamic equilibrium configuration of particles experiencing hydrodynamic drag forces in the normal direction is investigated. The forces affecting particle movement include the gravitational force $\mathbf{F}_{\mathrm{g}}$, buoyant force $\mathbf{F}_{\mathrm{b}}$, and hydrodynamic drag force $\mathbf{F}_{\mathrm{h}}$, which engender the normal transition probability (i.e., in the z-direction):

$$\mathbf{F}_{\mathrm{g}} = -\frac{4\pi}{3}a^3\rho_{\mathrm{p}}g\hat{\mathbf{z}} \tag{12}$$

$$\mathbf{F}_{\mathrm{b}} = +\frac{4\pi}{3}a^3\rho_{\mathrm{f}}g\hat{\mathbf{z}} \tag{13}$$

$$\mathbf{F}_{\mathrm{h}} = \frac{k_{\mathrm{b}}Tv(\eta)K^{-1}(\phi)}{D_{\mathrm{B}} + D_{\mathrm{si}}}\hat{\mathbf{z}} \tag{14}$$

where ρ_{p} and ρ_{f} are mass densities of particle and fluid, respectively, g is the gravitational acceleration, k_{b} is the Boltzmann constant, T is the absolute temperature, and $K(\phi)$ is the sedimentation coefficient. Heppel's sphere-in-cell model [25] is incorporated in this study to estimate the sedimentation coefficient (which decreases with respect to volume fraction) using

$$K^{-1}(\phi) = H(\phi) = \frac{6 + 4\phi^{5/3}}{6 - 9\phi^{1/3} + 9\phi^{5/3} - 6\phi^2} \tag{15}$$

The Brownian and shear-induced diffusivities [26] are represented as [17]

$$D_{\mathrm{B}} = \frac{k_{\mathrm{b}}T}{6\pi\mu a}S(\phi) \tag{16}$$

and

$$D_{\mathrm{si}} = \dot{\gamma}(\eta)a^2\hat{D}(\phi) \tag{17}$$

respectively, where $S(\phi)$ is a quantity related to the osmotic compressibility [26,30] dealing with increasing entropy with respect to the particle volume fraction. In this simulation study, $S(\phi)$ is, however, omitted:

$$D_{\mathrm{B}} \to \frac{k_{\mathrm{b}}T}{6\pi\mu a} \tag{18}$$

because the random trial movement implicitly includes the entropic contribution stemming from the configurational gradient of particles [29]. Among various results from experimental and

simulation studies on the functional form of $\hat{D}(\phi)$, we choose one widely accepted [5–7]:

$$\hat{D}(\phi) = \frac{1}{3}\phi^2\left(1 + \frac{1}{2}e^{8.8\phi}\right) \tag{19}$$

Detailed discussion about Eq. (14) and its application to colloidal filtration were presented elsewhere [26,31]. Note that the shear rate in Eq. (17) varies with the normal distance from the membrane surface, as defined in Eq. (8). The normal transition probability is then determined as

$$P_z = \min[1, \exp(-\beta\Delta E - \beta\lambda\mathbf{F}\cdot\Delta\mathbf{r})] \tag{20}$$

where $\beta = 1/k_bT$, $\lambda(=0.5)$ is the well known parameter of the force bias Monte Carlo simulation [32,33], $\Delta\mathbf{r}(=\mathbf{r}_{new}-\mathbf{r}_{old})$ is the random trial displacement, ΔE is in general the energy difference between the new and old particle positions, and $\mathbf{F}$ is the total force acting on each particle, i.e.,

$$\mathbf{F} = \mathbf{F}_g + \mathbf{F}_b + \mathbf{F}_h \tag{21}$$

Since this study targets hard spheres to investigate effects of Brownian and shear-induced diffusion on the critical flux, ΔE is always set to 0 unless particles overlap each other. When the particle moves from $\mathbf{r}_{old}$ to $\mathbf{r}_{new}$, a random number is generated (using FORTRAN 90 function `rand`), and is compared with the transition probability P_z. If the random number is less than or equal to P_z, then the trial movement is accepted, and the particle moves to the new position $\mathbf{r}_{new}$; otherwise, movement is rejected, and the particle stays at the old position $\mathbf{r}_{old}$. If the particle undergoes any overlap at $\mathbf{r}_{new}$ with another particle, the trial movement is immediately rejected because this situation is equivalent to $\Delta E \to \infty$, which is thermodynamically forbidden. Note that $\mathbf{r}_{new}$ is randomly selected using Eq. (9) with P_x, which already contains the axial bias and spatial homogeneity in the x- and y-directions, respectively, and its acceptance is subject to P_z. All the simulations use 2100 particles, and

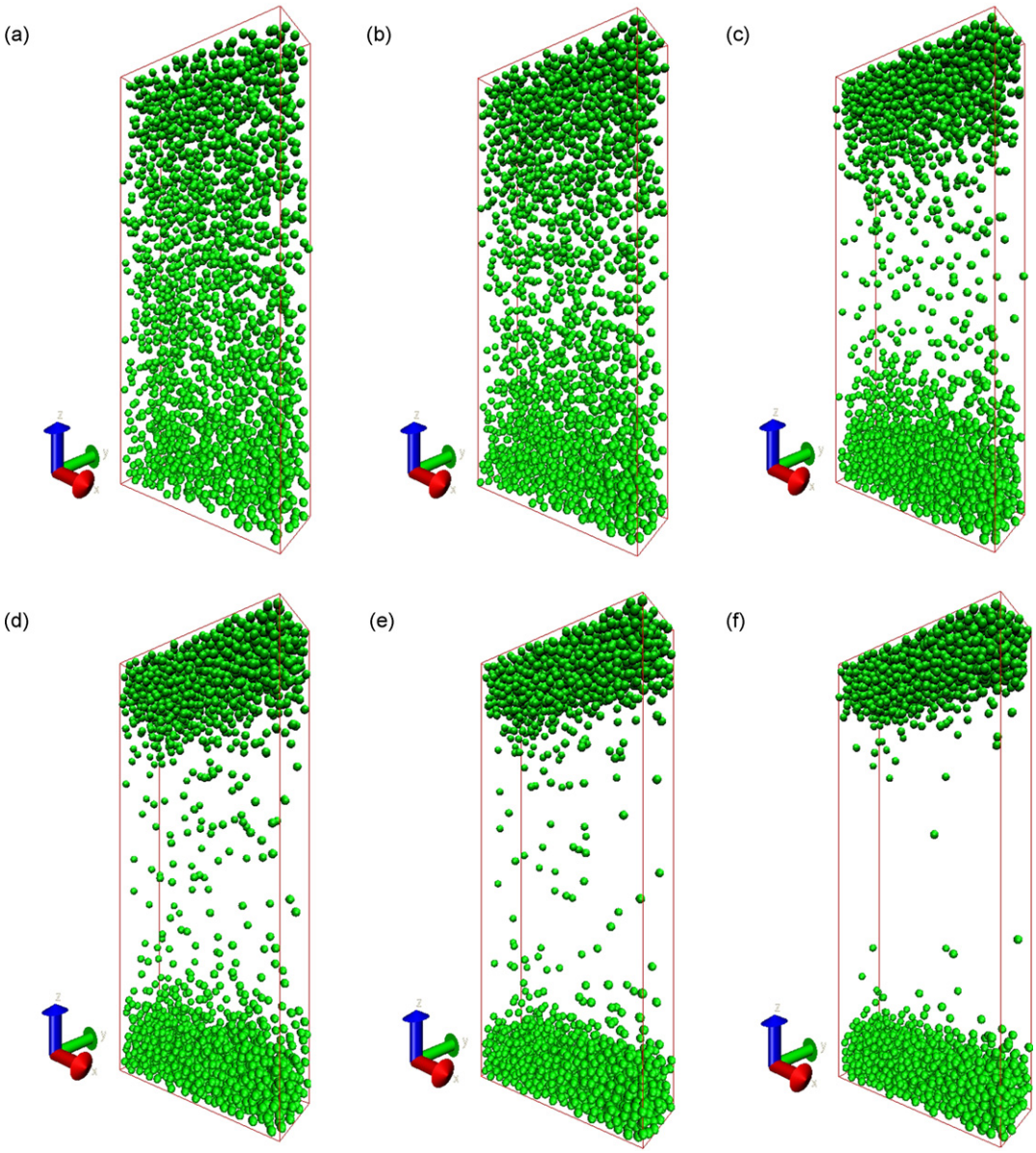

Fig. 3. Canonical MC simulations with the number of particles $N_p = 2100$, particle radius $a = 0.1$ μm, mass density $\rho_p = \rho_f$, and shear rate $\dot{\gamma} = 10^3\ s^{-1}$. The permeate flux v_w of simulations are (a) 0 μm/s, (b) 1 μm/s, (c) 5 μm/s, (d) 10 μm/s, (e) 20 μm/s, and (f) 30 μm/s.

in each MC cycle all the particles attempt to randomly move to new locations via the bias probabilities. The number of MC cycles is 1000, and statistical data are collected during the second half of the simulation. Due to the absence of strong pair-wise interparticle interactions, the filtration system rapidly converges to a dynamic equilibrium state within the first 500 MC cycles.

3. Results and discussion

3.1. Verification of transport mechanisms

Fig. 3 shows canonical MC simulations with various permeate flux values. In this simulation set, 2100 hard spheres are used to visually determine permeate flux that initiates or signifies polarized distribution of the particles in the simulation box. The initial volume fraction was set at 0.1, which seems to be excessive as a feed volume fraction; however, it rapidly starts pushing particles toward membrane surfaces using the inverse sedimentation coefficient of Eq. (15) and hence leaves a lesser number of particles near the epicenter of the membrane channel. Since the canonical ensemble is used in this study, the initial volume fraction is an important simulation factor. A smaller volume fraction close to the feed volume fraction would not provide meaningful results since the poverty of the particles in the membrane channel cannot render acceptable concentration gradients along the direction normal to the membrane surface. On the other hand, if the initial volume fraction is too high, then severe deposition will instantaneously occur through the sedimentation coefficient even with relatively low permeate fluxes, and the simulation may exaggerate serious fouling processes. Changing the total number of particles or altering the volume of the simulation box, given the permeate flux and shear rate, are possible alternatives, which are analogous to the grand canonical and isothermal–isobaric ensembles, respectively [29,34]. However, using these statistical ensembles in such a dynamic equilibrium state in a filtration system is a difficult task in terms of computation with dynamic memory allocation and analysis of stochastic data collected [35]. Adopting a consistent value of ϕ_{ini}, carefully chosen after preliminary tests, allows us to properly interpret simulation results and understand underlying physical meanings without extravagant trial-and-error parameterization.

Relatively homogeneous particle configuration is visually observed for $v_w = 0$ and $1\,\mu\text{m/s}$ as shown in Fig. 3(a) and (b), respectively. As the permeate flux increases, however, separation of particles into two major groups near double-membrane surfaces at $z = \pm h$ becomes apparent, as initiated at about $v_w = 5\,\mu\text{m/s}$, shown in Fig. 3(c). More realistic profiles of particle distribution along the direction normal to the membrane surface are shown in Fig. 3(d) and (e). Almost complete bisection of particle distribution is observed in Fig. 3(f), of which permeate flux of $30\,\mu\text{m/s}$ seems to cause significant fouling in terms of particle distribution along the vertical direction. Therefore, Fig. 3(a), (b), and (f) indicates that, using rough visual estimation, an optimal or critical flux will be located between 5 and $20\,\mu\text{m/s}$ (i.e., about 20 and $80\,\text{L/m}^2\,\text{h}$) for hard sphere suspensions. (A decisive method to quantify critical flux values is discussed in Section 3.2.) Local volume fractions near the epicenter can be interpreted as the feed volume fractions (see Fig. 4). It is worth noting that this range of fluxes, obtained by present MC simulations of non-interacting colloids of $0.1\,\mu\text{m}$, falls into the same range of experimental observations by multiple researchers with similar operating conditions [1,36,37].

Fig. 4 shows symmetric profiles of the volume fraction with different permeate fluxes. When the permeate flux is absent, the particles are almost homogeneously distributed throughout the

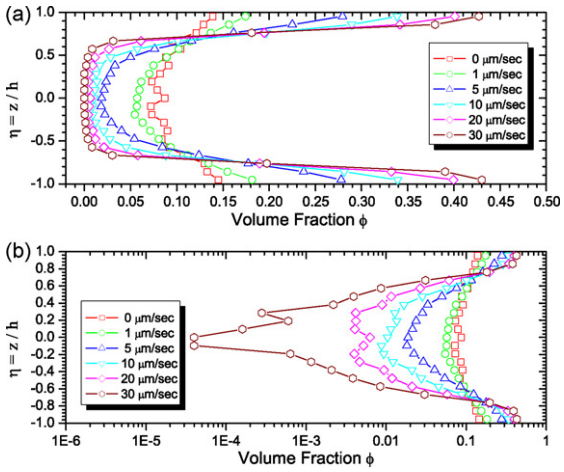

Fig. 4. Profiles of particle volume fractions in the normal direction with various permeate fluxes in (a) linear and (b) common-log scales of volume fraction. Particle radius is $0.1\,\mu\text{m}$, and shear rate is $1000\,\text{s}^{-1}$.

simulation box in comparison to cases of other non-zero permeate cases. However (slightly) higher concentration near the membrane surfaces (i.e., $\eta = \pm 1$) is observed, which may be attributed to the reflecting boundary condition under influences of the fast crossflow. This implies that, in concept, the wall concentration is always greater than the bulk concentration in the minimal presence of the permeate flux (even without any adsorption mechanisms) where the inertial lift is completely ignored. As the permeate flux increases, fewer particles stay near the epicenter, forming symmetric distributions. As indicated above, cases of $v_w = 10$ and $20\,\mu\text{m/s}$, which correspond to Fig. 3(d) and (e), can possibly be interpreted as crossflow filtration with feed volume fractions of $\phi_{\text{feed}} \simeq 0.01$ and 0.004 with the volume fraction on the membrane surface of $\phi_{\text{m}} \simeq 0.34$ and 0.40, respectively, which are less than the random packing ratio [38–40]. Fluctuations of volume fraction near the epicenter, observed when $v_w = 20$ and $30\,\mu\text{m/s}$, originate from the poverty of particles in the central region as visualized in Fig. 3(e) and (f). In addition, the symmetric distribution in the normal direction is conserved during the simulation, which confirms that the initial allocation of particles within the simulation box is close to purely random and sufficiently uniform.

Fig. 5 (with $\dot{\gamma} = 5000\,\text{s}^{-1}$) has very similar patterns of particle distribution along the direction normal to the membrane surface to those of Fig. 4 (with $\dot{\gamma} = 1000\,\text{s}^{-1}$), whilst other parameters used are same. It indicates that higher shear rates (i.e., $\dot{\gamma} = 5000\,\text{s}^{-1}$) alleviate particle deposition (accumulation) on the membrane surface, resulting in smaller values of volume fraction on the membrane surface. Experimental observations of similar behaviors were reported elsewhere [41]. Note that $v_w = 20$ and $30\,\mu\text{m/s}$ in Fig. 4 cause $\phi_{\text{m}} = 0.40$ and 0.43 on the membrane surfaces, respectively, when the same permeate fluxes in Fig. 5 engenders $\phi_{\text{m}} = 0.325$ and 0.362 with the larger shear rate. This comparison confirms that the effective force, derived as Eq. (14), decidedly represents the relative significance of shear-induce diffusion to Brownian diffusion by showing that higher shear alleviates the concentration polarization; however, it also implies that impacts of shear-rate on the particle deposition are mild for submicron-sized particles in terms of the wall concentration [1].

It is now worth re-noting that in Figs. 3–5, the underlying physics does not include the inertial lift phenomena [8–12] and its implications on the crossflow filtration [13]. The homogeneous distributions of particles with zero or negligible permeate flux may not be apparent due to the 'tubular pinch' effect. Particle

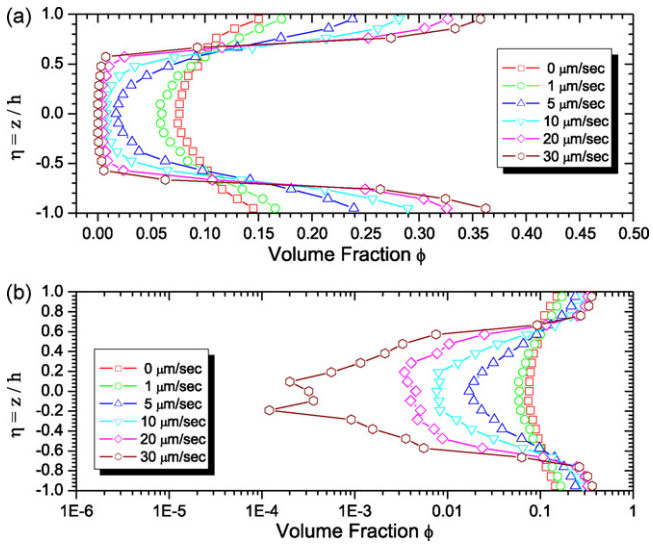

Fig. 5. Profiles of particle volume fractions in the normal direction with various permeate fluxes in (a) linear and (b) common-log scales of volume fraction. Particle radius is 0.1 μm, and shear rate is 5000 s^{-1}.

concentration would be inhomogeneous depending on the crossflow velocity, and therefore the concentration will vary along the normal distance from the channel wall (or membrane surface). The concentration at the epicenter might be different from the feed concentration, as implied by Segre and Silberberg's original work [8]. Phenomenologically, the inertial lift is proportional to the square of the shear rate and the cube of the particle radius, which must be significant for fast flow (of an order of (at least) 1 m/s) and large particles of sub-millimeter size. However, the inertial lift effects in a concentrated particle suspension is so far not well studied as to its importance in crossflow membrane filtration. In this light, the analyses of Figs. 3–5 are entirely based on Brownian and shear-induced diffusion whichever assumed to be major unified collective transport mechanisms.

3.2. Order parameter

The capability of the HFBMC method developed in this study was tested by showing the spatial distribution of particles. Particles are subject to the two orthogonal biases in the tangential and normal directions, quantified as P_x and P_z, respectively. The effective force derived as Eq. (14) rigorously captures the mitigating impact of the shear flow on the downward hydrodynamic drag forces exerted on particles. The range of fluxes that approximately border uniform and bisected particle distributions were roughly estimated on the visual basis.

At this stage, a particular physical quantity that can provide a rigorous tool to determine the critical flux is of great necessity. This quantity is often called an *order parameter* in statistical physics, which is used to denote "a fluctuating variable of which the average value provides a signature of the ordered state (or broken symmetry) in the system" [42]. The order parameter is a microscopic characteristic, conveniently chosen to be the difference in density or concentration between two phases. The "order" generally indicates a thermodynamic state rather than a (perfect) structural arrangement of solid cubics. In colloidal science, the concept of order parameter was widely used to investigate static and dynamic states of colloidal suspensions such as dynamical arrest and glass-formation [43], elastic colloidal stabilization through the nematic-isotropic structural transition [44], self-assembled nematic colloidal crystals [45], and jamming transition [46]. The above studies defined and used specific order parameters to represent structural phase transition of colloidal suspensions.

An order parameter in crossflow filtration, once chosen, should be (easily) calculable during the course of the HFBMC simulations and be available to extract physically meaningful information for determining the critical flux. We propose that the variance of particle locations (i.e., spatial distribution) as the order parameter for crossflow filtration:

$$\Psi = \frac{\langle (z-\bar{z})^2 \rangle}{h^2} = \frac{1}{N_p} \sum_{i=1}^{N_p} \left(\frac{z_i - \bar{z}}{h} \right)^2 \tag{22}$$

where z_i is the z-coordinate of the ith particle, and $\bar{z}$ is the mean z-coordinate of the N_p particles. For a completely homogeneous (aligned) distribution, i.e., $\phi(x, y, z) =$ constant, Ψ converges to 1/3 as proven below:

$$\Psi \simeq \frac{1}{N_p} \sum_{i=-N_p/2}^{N_p/2} \left(\frac{\delta z}{h} \right)^2 i^2 \simeq \left(\frac{N_p \delta z}{2h} \right)^2 \frac{1}{3} \simeq \frac{1}{3} \tag{23}$$

where $z_i = i(\delta z)$, and δz is the normal distance between the two nearest neighbors in the ideally aligned configuration. In a crossflow system, a permeate flux brings particles toward the membrane surfaces, indicating that more particles are located close to the membrane surfaces in comparison to the case of zero or negligible permeate flux. For vertically symmetric configurations of the buoyant particles (i.e., $\rho_p = \rho_f$) as shown in Fig. 3, the mean value of z-coordinates is close to 0 (i.e., $\bar{z} \simeq 0$), and the presence of particles near the membrane surfaces explicitly contributes to increasing Ψ from its minimum value of 1/3 to unity corresponding to the complete bisection. Therefore, the order parameter defined in Eq. (22) is bound between 1/3 and 1, which is valid only when the inertial lift is presumably neglected.

A set of simulation results in Fig. 6 shows variation of Ψ with respect to the permeate flux v_w. A total of 12 values of the permeate flux were chosen at 0.0 and 5 μm/s, and from 10 to 100 μm/s in intervals of 10 μm/s. A wide range of particle sizes (diameters) were tested from 0.1 to 10 μm. Each point of Fig. 6 represents one simulation using 2100 particles and 1000 MC cycles. It is observed that Ψ for smaller particles shows steep increase at the flux range of 0–20 μm/s, but remains on a plateau at the high flux region

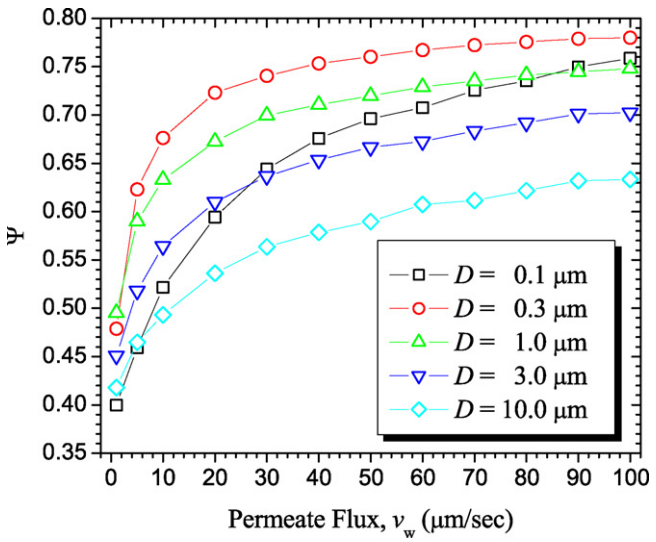

Fig. 6. The order parameter defined in Eq. (22) vs. the permeate flux. The order parameter increases with v_w and decreases with the particle diameter (excluding $D = 0.1$ μm case). The shear rate used for these simulations is $\gamma_0 = 3.33 \times 10^3$ s^{-1}.

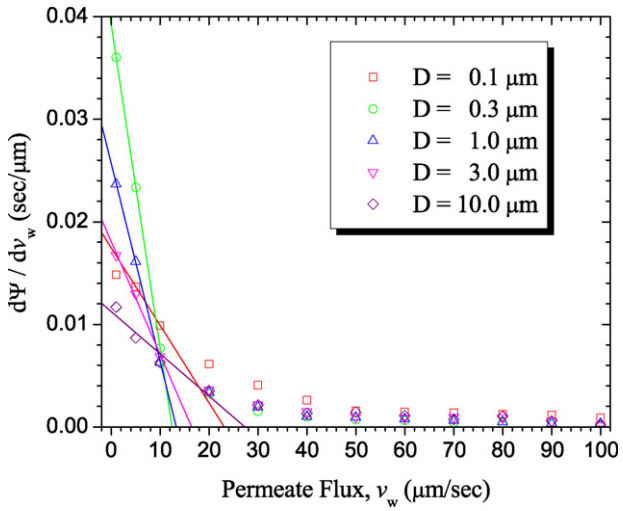

Fig. 7. The derivative of the order parameter with respect to the permeate flux obtained from Fig. 6. Each line indicates the linear regression using the first few data points from $v_w = 0$. Abscissas of the linear regression lines (i.e., x-intercepts of regressed lines) point out critical fluxes based on the asymptotic discontinuity of the order parameter, resembling that of the second-order phase transition.

close to 100 μm/s. This trend of rapid increase of Ψ at low fluxes attenuates as the particle size increases from 0.3 to 10.0 μm. In general, increase in Ψ indicates that more particles stay away from the channel epicenter, and so the particle distribution deviates from the homogeneity of the initial configuration. It is worth noting that Ψ values in Fig. 6 are all greater than 1/3, indirectly confirming that the order parameters were appropriately calculated. Moreover, the deviation of Ψ from 1/3 of zero flux indicates that the wall concentration is higher than the bulk concentration as discussed in Section 3.1. This phenomena is important only when the feed volume fraction is about or more than a few percent (volume to volume) because the particles loose their degree of freedom in their movements near the membrane surface, which plays the role of a geometrical barrier.

The behavior of 0.1 μm particle in terms of Ψ is very different from that of other bigger particles. While the other four Ψ curves are clearly stratified in an organized manner with respect to the particle size, Ψ of diameter $D = 0.1$ μm generates cross-points with most other curves, diverts from the stratification propensity, and hence implies that the filtration of 0.1 μm particles follows a different transport mechanism from that of the four others. Therefore, it can be inferred that at about $D \simeq 0.3$ μm exists delimitation between Brownian and shear-induced diffusion with the shear rate of 3333 s^{-1}. Different values of shear rates will change the magnitude and variation of Ψ with respect to v_w, but we selected this shear rate (i.e., 3333 s^{-1}) to compare our simulation results with reported experimental observations.

It is assumed that Ψ contains information on structural characteristics that is fundamentally related to the critical flux. Close investigation of Fig. 6 allows us to recognize that there are two distinct regions in terms of variational behavior of Φ: regimes of acclivity and plateau at low and high fluxes, respectively. However, the variation of Φ is rather smooth and therefore not enough to determine a point of permeate flux that can clearly discriminate two different phases of particle distributions, i.e., in essence uniform and conspicuously bisected. Therefore, Ψ of Fig. 6 is numerically differentiated with respect to v_w, and the results are shown in Fig. 7. As expected, $d\Psi/dv_w$ is high for low fluxes, and vice versa. A higher value of $d\Psi/dv_w$ indicates the sensitive changes of Ψ with respect to v_w, and negligible $d\Psi/dv_w$ means a minute change in structures. The offset of $d\Psi/dv_w$ on the v_w-axis is, however, not clear in Fig. 7, so a linear regression is performed using the first points of each curve. The dotted lines show the linear regression plots, and their x-intercepts asymptotically delineate transition points of $d\Psi/dv_w$ from finite to vanishing values. Therefore, each curve of Fig. 7, seeming to vary in a power-wise manner, can be divided into two regions of linear decline and zero slope. Offset points can be interpreted as fluxes of phase transition, the trend of which is analogous to the second-order phase transition [42], in which the second-order derivative of the order parameter is discontinuous near the transition point. The variation of $d\Psi/dv_w$ can be then simplified as

$$\frac{d\Psi}{dv_w} = \begin{cases} -C_1 v_w + C_2 & \text{for } v_w < J_{crit} \\ 0 & \text{for } v_w > J_{crit} \end{cases} \quad (24)$$

where C_1 and C_2 are constants to be determined using the linear regression, $J_{crit}(= C_1/C_2)$ is defined as the permeate flux at which $d\Psi/dv_w$ vanishes at first as v_w increases from 0. Note that the derivative of Eq. (24), i.e., the second-order derivative of the (linearized) order parameter, Ψ, gives a mathematically discontinuous point at $v_w = J_{crit}$. In this way, we approximately use the method of determining the critical point of the second-order phase transition to estimate the critical flux in the crossflow membrane filtration.

3.3. Critical flux

The critical flux J_{crit} determined using Eq. (24) is plotted in Fig. 8 with respect to the particle diameter in comparison to Kwon et al.'s experimental observations [36]. Note that determination of one value of critical flux shown in Fig. 8 requires a series of simulations with a fixed value of particle diameter and various permeate fluxes for the phase transition analysis using Eq. (24). The total number of simulations performed to obtain the critical fluxes of Fig. 8 is 60 for five different particle diameters with 12 permeate fluxes each.

Experimental work performed by Kwon et al. is summarized as follows: they determined critical fluxes using two different methods in terms of particle mass balance (PMB) and TMP.

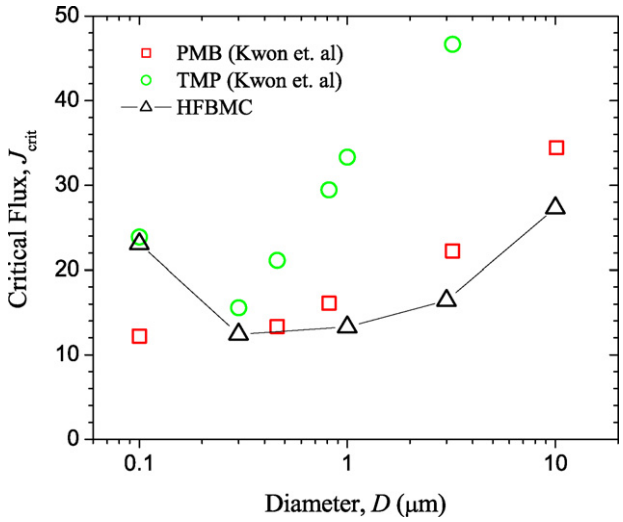

Fig. 8. Comparison of critical fluxes of HFBMC simulations and experimental observations by Kwon et al. [36] using particle mass balance (PMB) and transmembrane pressure (TMP) methods. Operational conditions are as follows: crossflow $\bar{u} = 0.2$ m/s, ionic strength $IS = 10^{-5}$ M, and temperature $T = 25$ °C. The length, width, and height of the membrane channel are 60, 6, and 0.36 mm, respectively. The estimated shear rate is $\gamma_0 = 3.33 \times 10^3$ s^{-1}.

(1) "**Based on particle mass balance.** By monitoring the change of particle concentration in the fluid phase, the extent and rate of particle deposition at membrane surfaces can be determined at various permeation rates. The highest flux value at which no particle deposition is observed, is taken as the critical flux."
(2) "**Based on the increase in TMP** required to maintain a constant permeate flux. The TMP increases during the constant permeate flux operation in order to compensate for the increase in the resistant to permeation. Accordingly, the critical flux is the flux below which there is no presence of this increase in resistance to permeation (i.e., the TMP is constant with time)."

It is worth remarking that critical fluxes, predicted using our MC simulations and measured by Kwon et al. using the PMB method, show reasonably good agreements for particles greater than 0.3 μm. The particle deposition defined above is based on the timely change of concentration in the feed solution of a close-looped filtration unit, which shows less than 1% of change with zero suction (no permeation) during the first 50 min [36]. Therefore, the concentration of the feed solution decreases as the permeate flux increases. Interactions between particles and the membrane can contribute to the initial deposition, forming the first and next deposition layers on the membrane surface, assuming that the particles overcome the primary potential peak of the particle–membrane interaction [47]. The next accumulation is mainly influenced by the permeate flux, which brings particles down to the membrane surface, causing the concentration polarization. Amounts of accumulated particles contributing to the variation of feed solution may not be purely from the first layers of the particle deposition, but stationary formation of the concentration polarization. We assume that Kwon et al.'s PMB method incorporates the general concept of particle accumulation on the membrane surface, possibly including sticking of particles on the membrane surface through particle–membrane interaction (forming the first layers) and post-formation of stationary concentration polarization that contributes to the decrease in feed concentration. Our HFBMC predicts slightly lower critical fluxes than their PMB-based flux values, which can be explained in terms of interparticle interactions. The ionic strength used in their experiments is 10^{-5} M, where colloidal particles are usually repulsive if their zeta potential is of an order of O(10) mV in magnitude. Repulsive interparticle interactions mitigate the particle deposition, attenuate structural bisection (i.e., concentration polarization), and so reduce values of the order parameter. In other words, stronger repulsion between particles allows higher critical flux below which no fouling occurs.

As noted above, the goal of the current study is to delineate in a consistent way a baseline of the critical flux using the non-interacting hard spheres undergoing Brownian and shear-induced diffusion only, i.e., pure equilibrium thermodynamic and non-equilibrium hydrodynamic origins, respectively [26]. Without enough shear rate (subject to the particle size), Eq. (14) implies that the critical flux must decrease with respect to increasing particle size since larger particles will undergo stronger hydrodynamic drag forces toward the membrane surface. Stronger shear enhances back-diffusion of (larger) particles from the membrane surface to the bulk phase even though their Brownian diffusion is negligible. The HFBMC results shown in Fig. 8 indicate that the critical flux of repulsive particles is higher than that of hard spheres larger than an order of $O(10^{-1})$ μm with shear rate of an order of $O(10^3)\,s^{-1}$. Comparison of the critical fluxes measured indicates that TMP estimation always provides higher critical flux than that gauged using the PMB method, which may indicate two distinct stages in the critical flux determination in terms of static distribution and dynamic deposition for PMB and TMP, respectively.

The PMB result is close to the current HFBMC simulation because both deal with concentration polarization (i.e., spatial deviation of particle distribution away from the uniform configuration) as a main criteria to determine the critical flux. The highest flux that initiates particle deposition (accumulation) in experiments corresponds to the flux that makes a transition of $d\Phi/dv_w$ from the rapid (almost) linear decrease to the indifferent variation, as shown in Fig. 7. The PMB and HFBMC both represent the first steady state near which the initial, noticeable concentration polarization occurs with abrupt spatial bias of the particle distribution. Therefore, the hydrodynamics (i.e., convective drag force) and reversible/irreversible thermodynamics (i.e., Brownian/shear-induced diffusion) are appropriately balanced in the steady state. In this light, the critical flux estimated by the TMP method indicates an irreversible thermodynamic state in which diffusion is drastically suppressed by permeation. Due to the unceasing increase in TMP (above the critical flux), the TMP critical flux may possibly indicate another transition from quasi-equilibrium to pure dynamic (non-equilibrium) thermodynamic state, which is however out of the scope of the current study.

It is interesting to see that the HFBMC critical flux shows excellent agreement with experimental TMP critical flux for 0.1 μm particles, of which shear-induced diffusion seems to be insignificant. This case corresponds to our previous study that defines the critical flux based on liquid to solid transition [23]. In the normal direction, Brownian diffusion and hydrodynamic drag of 0.1 μm particles are balanced with negligible shear effects, and the crossflow primarily contributes to the tangential transport, which leads to a steady state. This implies that the HFBMC fundamentally predicts TMP and PMB critical fluxes where Brownian and shear-induced diffusion are dominant, respectively. In addition, it is worth noting that the pore size of MF membrane used in Kwon et al.'s work is 0.2 μm, in which 0.1 μm diameter particles can easily cause surface pore blocking or internal fouling. This can explain why the PMB critical flux of 0.1 μm diameter particles is less than that of our simulation results (Fig. 8). The presence of a minimum critical flux with respect to the particle size corresponds to different back-transport mechanisms of polydispersed particles during filtration, validating the concept of a minimum in particle diffusivity [48,49]. A (much) larger-scale simulation with accurate hydrodynamics (such as Stokesian dynamics) are of great necessary for further investigation dealing with particle motions near membrane pores [50,51] as indicated by Kwon et al. [36].

4. Conclusions

The HFBMC was developed to investigate the crossflow filtration of colloidal hard spheres undergoing both Brownian and shear-induced diffusion simultaneously. An effective hydrodynamic drag force acting on a hard sphere in a concentrated shear flow within a membrane channel is incorporated into the HFBMC simulations. Transition probability is composed of tangential and normal biases, which are based on the axial convection and the vertical drag force, respectively. Results of critical flux from the HFBMC using non-interacting hard spheres follow the same experimental propensity of those estimated using the PMB method [36]. This is because the experimental and simulation approaches are based on formation of the concentration polarization, causing the initial deposition of particles, characterized by the biased distribution. The TMP method can be inferred to provide a transition point to a pure non-equilibrium (dynamic) state, which requires further extensive investigation. The HFBMC resulted in better agreements with TMP and PMB critical fluxes for smaller (< 0.3 μm) and larger (> 0.3 μm) particles, respectively, discriminating the dominant diffusion mechanisms.

Acknowledgments

This research was made possible by a grant from the US National Science Foundation Faculty Early Career (CAREER) Development Program (CTS04-49431), the Engagement Grant between Maui High Performance Computing Center and the University of Hawaii, High School Intern Program of the College of Engineering in the University of Hawaii, and Saehan Industries, Seoul, Korea. We thank two students, Steven Bartz from Philip Academy, Andover, Massachusetts and Rentaro Matsukata from Punahou High School, Honolulu, Hawaii for volunteering as interns to work on parallel computing using MPI and scientific visualization using Virtual Molecular Dynamics (VMD) in summer 2007.

References

[1] R.D. Cohen, R.F. Probstein, Colloidal fouling of reverse osmosis membranes, Journal of Colloid and Interface Science 114 (1) (1986) 194–207.
[2] R.W. Field, D. Wu, J.A. Howell, B.B. Gupta, Critical flux concept for microfiltration fouling, Journal of Membrane Science 100 (3) (1995) 259–272.
[3] P. Bacchin, P. Aimar, R. Field, Critical and sustainable fluxes: theory, experiments and applications, Journal of Membrane Science 281 (1–2) (2006) 42–69.
[4] A. Einstein, Investigation on the Theory of the Brownian Movement, Dover Publications, Inc., New York, 1956.
[5] D. Leighton, A. Acrivos, Measurement of the shear induced coefficient of self-diffusion in concentration suspensions of spheres, Journal of Fluid Mechanics 177 (1987) 109–131.
[6] D. Leighton, A. Acrivos, The shear-induced migration of particles in concentrated suspensions, Journal of Fluid Mechanics 181 (1987) 415–439.
[7] D. Leighton, A. Acrivos, Viscous resuspension, Chemical Engineering Science 41 (6) (1986) 1377–1384.
[8] G. Segre, A. Silberberg, Radial particle displacements in Poiseuille flow of suspensions, Nature 189 (21) (1961) 209–210.
[9] D.A. Drew, J.A. Schonberg, G. Belfort, Lateral inertial migration of a small sphere in fast laminar flow through a membrane duct, Chemical Engineering Science 46 (12) (1991) 3219–3224.
[10] F.W. Altena, R.J. Weigand, G. Belfort, Lateral migration of spherical particles in laminar porous tube flow: application to membrane filtration, PhysicoChemical Hydrodynamics 6 (1985) 393–413.
[11] F.W. Altena, G. Belfort, Lateral migration of spherical particles in porous channels: application to membrane filtration, Chemical Engineering Science 39 (1985) 343–355.
[12] J.R. Otis, F.W. Altena, J.T. Mahar, G. Belfort, Measurements of single spherical particle trajectories with lateral migration in a slit with one porous wall under laminar flow conditions, Experiments in Fluids 4 (1) (1986) 1–10.
[13] S. Chellam, M.R. Wiesner, Particle transport in clean membrane filters in laminar flow, Environmental Science and Technology 26 (8) (1992) 1611–1621.
[14] P. Bacchin, P. Aimar, V. Sanchez, Model for colloidal fouling of membranes, AIChE Journal 41 (2) (1995) 368–376.
[15] C.A. Romero, R.H. Davis, Transient model of crossflow microfiltration, Chemical Engineering Science 45 (1990) 13–25.
[16] L.F. Song, M. Elimelech, Theory of concentration polarization crossflow filtration, Journal of Chemical Society, Faraday Transactions 91 (1995) 3389–3398.
[17] S. Sethi, M.R. Wiesner, Modeling of transient permeate flux in cross-flow membrane filtration incorporating multiple particle transport mechanisms, Journal of Membrane Science 136 (1997) 191–205.
[18] R. Chan, V. Chen, The effects of electrolyte concentration and ph on protein aggregation and deposition: critical flux and constant flux membrane filtration, Journal of Membrane Science 185 (2) (2001) 177–192.
[19] V. Chen, A.G. Fane, S. Madaeni, I.G. Wenten, Particle deposition during membrane filtration of colloids: transition between concentration polarization and cake formation, Journal of Membrane Science 125 (1) (1997) 109–122.
[20] A.S. Kim, S. Bhattacharjee, M. Elimelech, Shear-induced reorganization of deformable molecular assemblages: Monte Carlo studies, Langmuir 17 (2001) 552–561.
[21] G. Arya, A.Z. Panagiotopoulos, Monte Carlo study of shear-induced alignment of cylindrical micelles in thin films, Physical Review E (Statistical, Nonlinear and Soft Matter Physics) 70 (3) (2004) 031501.
[22] J.C. Chen, A.S. Kim, Review of Brownian dynamics, molecular dynamics and Monte Carlo modeling of colloidal systems, Advances in Colloid and Interface Science 112 (1–3) (2004) 159–173.
[23] J.C. Chen, M. Elimelech, A.S. Kim, Monte Carlo simulation of colloidal membrane filtration: model development with application to characterization of colloid phase transition, Journal of Membrane Science 255 (2005) 291–305.
[24] J.C. Chen, A.S. Kim, Monte Carlo simulation of colloidal membrane filtration: principal issues of modeling, Advances in Colloid and Interface Science 119 (2006) 35–53.
[25] J. Happel, Viscous flow in multiparticle systems: slow motion of fluids relative to beds of spherical particles, AIChE Journal 4 (1958) 197–201.
[26] A.S. Kim, Y. Liu, Irreversible chemical potential and shear-induced diffusion in crossflow filtration, Industrial & Engineering Chemical Fundamentals, doi:10.1021/ieø7144ø3, in press.
[27] W. Gropp, E. Lusk, A. Skjelum, Using MPI: Portable Parallel Programming with the Message-Passing Interface, The MIT Press, Cambridge, Massachusetts, 1997.
[28] A.S. Berman, Laminar flow in channels with porous walls, Journal of Applied Physics 24 (9) (1953) 1232–1235.
[29] M.P. Allen, D.J. Tildesley, Computer Simulation of Liquids, Oxford Science Publications, Oxford, UK, 1987.
[30] J.P. Hansen, I.R. McDonald, Theory of Simple Liquids, Academic Press, London, 1976.
[31] A. Sierou, J.F. Brady, Shear-induced self-diffusion in non-colloidal suspensions, Journal of Fluid Mechanics 506 (2004) 285–314.
[32] M. Rao, B.J. Berne, On the force-bias Monte Carlo simulation of simple liquid, Journal of Chemical Physics 71 (1979) 129–132.
[33] M.P. D'evelyn, S.A. Rice, Comment on the configuration space diffusion criterion for optimization of the force bias Monte Carlo method, Chemical Physics Letters 77 (3) (1981) 630–633.
[34] A.S. Kim, E.M.V. Hoek, Cake structure in dead-end membrane filtration: Monte Carlo simulation, Environmental Engineering Science 19 (6) (2002) 373–386.
[35] G. Redwine, Upgrading to FORTRAN 90, Springer-Verlag, New York, 1995.
[36] S. Kwon, D.Y. Vigneswaran, A.G. Fane, R.B. Aim, Experimental determination of critical flux in cross-flow microfiltration, Separation and Purification Technology 19 (3) (2000) 169–181.
[37] S. Milcent, H. Carrere, Clarification of lactic acid fermentation broths, Separation and Purification Technology 22–23 (3) (2001) 393–401.
[38] G.T. Nolan, P.E. Kavanagh, Computer simulation of random packing of hard spheres, Powder Technology 72 (1992) 149–155.
[39] G.Y. Onoda, E.G. Liniger, Random loose packing of uniform spheres and the dilantancy onset, Physical Review Letters 64 (22) (1990) 2727–2730.
[40] W. Soppe, Computer simulation of random packings of hard spheres, Powder Technology 62 (1990) 189–196.
[41] S. Chellam, M.R. Wiesner, Evaluation of crossflow filtration models based on shear-induced diffusion and particle adhesion: complications induced by feed suspension polydispersivity, Journal of Membrane Science 138 (1) (1998) 83–97.
[42] J.-L. Barrat, J.-P. Hansen, Basic Concepts for Simple and Complex Liquids, Cambridge University Press, New York, 2003.
[43] K.A. Dawson, P. De Gregorio, A. Lawlor, Dynamically arrested states of matter, Advances in Colloid and Interface Science 122 (1–3) (2006) 35–38.
[44] P. Galatola, J.B. Fournier, Nematic-wetted colloids in the isotropic phase: pairwise interaction, biaxiality, and defects, Physical Review Letters 86 (17) (2001) 3915–3918.
[45] I. Musevic, M. Skarabot, U. Tkalec, M. Ravnik, S. Zumer, Two-dimensional nematic colloidal crystals self-assembled by topological defects, Science 313 (5789) (2006) 954.
[46] V. Trappe, V. Prasad, L. Cipelletti, P.N. Segre, D.A. Weitz, Jamming phase diagram for attractive particles, Nature 411 (2001) 722.
[47] P. Bacchin, P. Aimar, V. Sanchez, Influence of surface interaction on transfer during colloid ultrafiltration, Journal of Membrane Science 115 (1) (1996) 49–63.
[48] S. Chellam, M.R. Wiesner, Particle back-transport and permeate flux behavior in crossflow membrane filters, Environmental Science & Technology 31 (3) (1997) 819–824.
[49] M.R. Wiesner, M. Clark, J. Mallevialle, Membrane filtration of coagulated suspensions, Journal of Environmental Engineering 115 (1) (1988) 20–40.
[50] M.M. Kim, A.L. Zydney, Particle–particle interactions during normal flow filtration: model simulations, Chemical Engineering Science 60 (15) (2005) 4073–4082.
[51] M.M. Kim, A.L. Zydney, Theoretical analysis of particle trajectories and sieving in a two-dimensional cross-flow filtration system, Journal of Membrane Science 281 (1–2) (2006) 666–675.